



Analysis of the coaxiality–geometric hysteresis model of a rotate vector reducer based on Ansys Adams

Yongming Liu¹, Lei Fu^{1,3}, Zhuanzhe Zhao¹, Qiang Ma¹, Yujian Rui^{1,2}, and Zhen Zhang¹

¹School of Mechanical Engineering, Anhui Polytechnic University, Wuhu, Anhui 241000, China

²Wuhu Ceprei Robot Technology Research Co., Ltd., Wuhu, Anhui 241003, China

³BOZHON Precision Industry Technology Co., Ltd., Suzhou, Jiangsu 215200, China

Correspondence: Zhuanzhe Zhao (zhuanzhe727@ahpu.edu.cn)

Received: 6 February 2022 – Revised: 17 August 2022 – Accepted: 1 September 2022 – Published: 13 October 2022

Abstract. When a traditional performance test device, the rotate vector (RV) reducer, is loading and unloading the reducer tested or running in different torque ranges, the coaxiality error generated by the transmission system has an important impact on the detection accuracy of a key performance parameter of the RV reducer, the hysteresis. In order to design a high-precision performance test device, a RV reducer coaxiality–geometric hysteresis model is proposed. First of all, the static simulation analysis of the transmission system of the traditional performance test device in different torque ranges is carried out using Ansys software, and the corresponding coaxiality error is obtained. Secondly, the RV reducer coaxiality–geometric hysteresis model is established by means of geometric analysis, and combined with Adams dynamics simulation software, the dynamic simulation analysis is carried out under the condition that the coaxiality of the model transmission system is in different error ranges and has no load. When the coaxiality is within the allowable error range, the hysteresis value is 0.5467 arcmin, and the result shows that the accuracy of the model is verified. At the same time, when the coaxiality exceeds the allowable range of error, it will have a great impact on the hysteresis. This result has certain theoretical significance and practical value for the analysis of the influence of the coaxiality error of the high-precision RV reducer performance detection device and the design of the adjustment mechanism.

1 Introduction

The rotate vector reducer has a series of advantages such as small size, light weight, large transmission ratio range, long life, high precision, high efficiency, and stable transmission and has been widely used in industrial robots, CNC (computer numerical control) machine tools, and other fields (Yu et al., 2017; Qian et al., 2020; Wang et al., 2019). Hysteresis is one of the most important technical parameters and indicators in the application of RV reducers (Pham and Ahn, 2017; T. Li et al., 2020). Due to confidentiality and other reasons, it is difficult to obtain technical data, which brings certain difficulty to the theoretical calculation. At the same time, the hysteresis parameters calculated by theory are often limited by various factors and can only be used as reference values. Therefore, scholars at home and abroad put forward many methods and factors to calculate and influence hysteresis, and some achievements are as follows: Tran et

al. (2016) combined finite element and kinematics analysis to study the idling of the cycloidal pin gear reducer, first considering the effect of tolerance on the idling of the cycloidal pin gear reducer and then conducting an iterative finite element analysis of the idling of the cycloidal pin gear reducer. The results show that the lost motion of the cycloid reducer depends not only on its torsional stiffness but also its tolerance. T. Tang et al. (2021) proposed a new model to capture transmission compliance and hysteresis and its degradation. This phenomenon is represented by the combination of nonlinear stiffness components and micro-sliding friction in the tooth meshing area. The proposed model takes into account the interference effects of multi-tooth meshing and the reducer. The parameters of the model are determined using optimization techniques, and special harmonics are used. Numerical simulation and driving test equipment experimental data are compared to prove the proposed model. Bednarczyk (2021)

uses an output mechanism to transmit the driving force from the active side of the main rolling node gear of the cycloid reducer to the output side. And through the structure and geometry of the output mechanism, the backlash distribution in it is analyzed, while considering the formation of the machining deviations of the elements and surfaces of the mechanism, determining the distribution of forces and contact pressures. The analysis results show that the backlash distribution, force, and contact pressure are highly dependent on the bushing arrangement radius and the tolerance of the planetary gear bore. According to the elastic deformation theory of the thin shell, the principle of harmonic transmission and the source of the harmonic transmission error are analyzed, and the calculation of the transmission error is further discussed; the transmission error formula of the harmonic gear reducer considering the gear backlash and stiffness is given in Tong et al. (2013). The detection system of the transmission error of the gear reducer is designed for the first harmonic. The system realizes the detection of static and dynamic transmission errors of the harmonic gear reducer. Zou et al. (2015) propose a new harmonic drive model, which takes into account the geometry, internal interactions, and assembly errors of key parts; uses low-speed tests to fit kinematic errors; and analyzes its generation mechanism. Based on the new model, a speed step simulation, the new model reveals the dynamic behavior of harmonic drive systems, which will aid in the dynamic design and precise control of harmonic drive systems. T. Li et al. (2020) took the RV cycloid pin gear transmission as the research object, considered the influence of manufacturing errors, established the theoretical contact analysis model of the cycloid pin gear transmission, realized the effective pre-control of the tooth profile and meshing contact performance through the analysis, and verified the analysis results. These showed that the manufacturing error has a great influence on the transmission accuracy of the RV cycloid pin gear, and the pitch error has the greatest influence on the transmission error, which is directly proportional. The tooth profile error has a secondary effect on the transmission error. Ahn et al. (2021) considered the tolerance and friction between the cycloid and the needle, established the finite element model of the RV reducer and the eccentric shaft, and verified it through theoretical calculations. At the same time, they studied the tolerance and friction of the multi-contact RV, and the effect of the output torque of the reducer shows that the tolerance is mainly to reduce the torsional stiffness, while the friction mainly increases the fluctuation of the output torque. Based on the functional principle and the influence of wear, a performance margin model was established with hysteresis and transmission errors as the key performance parameters, and then the multi-source uncertainty was analyzed and quantified, including manufacturing errors, uncertainties in operating, and environmental conditions in Z. Li et al. (2020). And then the multi-source uncertainty was analyzed and quantified, including manufacturing errors, uncertainties in operation, uncertainty of the thresh-

old, and environmental conditions in Y. Li et al. (2020). The research results show that the proposed method can provide some suggestions for the design and manufacturing stage of the harmonic reducer.

The hysteresis generated during the rotary motion of the RV reducer and the test system is affected by various factors, and the position of the instantaneous rotary axis changes frequently. According to the principle of relative motion, at any instant, on the one hand the axis of rotation rotates around its own instantaneous axis of rotation. On the other hand, the instantaneous axis of rotation also moves axially, radially, and obliquely with respect to the ideal axis of rotation. The coaxiality error of the RV reducer and the test system is the maximum radial distance between the rotation axis and the reference axis, which will cause the rotation axis of the rotating shaft to deviate from the correct position, affecting the centering accuracy and orientation accuracy of the RV reducer and the testing system shafting, so that the hysteresis of the RV reducer and the test accuracy of the detection device have changed.

The research content in the above literature does not involve the influence of the geometric error of the coaxiality on the hysteresis of the RV reducer and its test accuracy. At the same time, the established model is too complicated, and the generalization ability is limited, which brings inconvenience to the actual RV reducer geometric hysteresis design, detection accuracy, and engineering application.

This paper takes the RV-20E reducer as a subject, establishes the coaxiality–geometric hysteresis model of the RV reducer, and conducts in-depth research on the influence of coaxiality error on RV reducer hysteresis and its test accuracy. Firstly, the coaxiality error of the transmission system of the traditional performance test device under different loads is analyzed by Ansys software; secondly, the coaxiality–geometric hysteresis model of the RV reducer is established by the method of geometric analysis, and the dynamic simulation analysis is carried out with Adams. The accuracy of the model is verified; at the same time, dynamic simulation analysis is carried out when the coaxiality of the model is within different error ranges and the output end has no load, and the influence of different coaxiality on the hysteresis is given. The coaxiality of the high-precision detection device for the performance of the reducer, the hysteresis of the RV reducer, and the design of its adjustment mechanism have certain theoretical significance and practical value.

2 Statics simulation based on Ansys

According to the RV reducer–transmission relationship, the geometric hysteresis of the RV reducer mainly consists of the following three parts: the geometric hysteresis of the gradient cylinder gear drive (primary deceleration), the geometric hysteresis of needle wheel planetary transmission (secondary deceleration), and the geometric hysteresis of the eccentric-



Figure 1. RV reducer performance parameter test device.

rotation arm bearing. Since each tooth surface of the reducer is rigidly engaged, the geometric hysteresis of the coaxiality of the RV-20E reducer is analyzed as follows.

2.1 Statics model based on the establishment of Ansys

The performance test device, the RV reducer, is a mechanical device used to detect key parameters such as the hysteresis value. As shown in Fig. 1, during the test process, the coaxiality error of the transmission system of the device will affect the RV reducer deceleration. In order to further explore the influence of the coaxiality error on the hysteresis of the RV reducer during operation, Ansys software was used to perform statics simulation analysis on the transmission system of the traditional RV reducer performance testing device, so as to obtain the possible coaxiality errors of the input shaft and output shaft of the RV reducer during the operation of the transmission system (Yang et al., 2019; Gao et al., 2012; Su et al., 2020); the model building steps are as follows.

2.1.1 Simplified transmission system model

First of all, the RV reducer performance testing device was established with a 3D solid model through SolidWorks, and then unnecessary parts were removed, such as the support, base, and slider, leaving the parts required for the transmission system. The simplified model is shown in Fig. 2.

2.1.2 Parameter setting of non-mechanical parts of the transmission system

Since non-mechanical parts belong to the instrument category, specific material properties cannot be given, so materials are added according to the principle of equal mass conversion. The specific parameters are shown in Table 1.

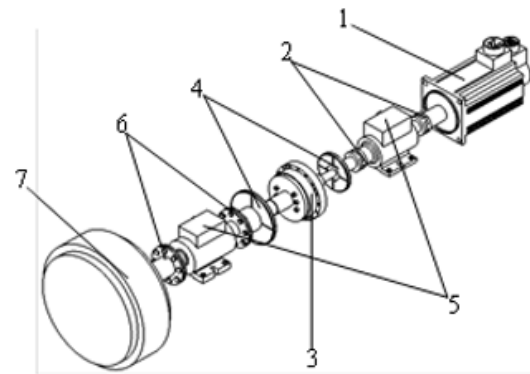


Figure 2. Simplified model of transmission system: (1) servo motor, (2) plum blossom coupling, (3) RV reducer, (4) raster encoder, (5) torque sensor, (6) diaphragm coupling, and (7) magnetic powder brake.

2.1.3 Material parameter setting of mechanical parts of the transmission system

The material properties of the mechanical parts of the transmission system are added, and the specific parameters are shown in Table 2.

2.1.4 Setting of boundary conditions of transmission system

Figure 3 shows the setting of the boundary conditions of the simplified model in Ansys software. The specific parameters are shown in Tables 3 and 4. Table 3 shows the boundary gravity of mechanical and non-mechanical transmission systems when $g = 9.8 \text{ m s}^{-2}$. The non-mechanical parts are fixed on the base, so they are subjected to reaction force. The boundary torque in Table 4 is the range of the torque sensor selected during actual measurement.

2.2 Ansys simulation results

Through Ansys to analyze the input shaft and output shaft of the transmission system, the cloud displacement path change in the y direction can be obtained. This article takes a set of boundary conditions in Table 4 (input shaft $T_1 = 1.43 \text{ Nm}$, output shaft $T_2 = 200 \text{ Nm}$) as an example. After analysis, the simulation effect is shown in Fig. 4, and the radial displacement change is shown in Fig. 5.

The tilt model of the input and output drive shafts from Fig. 4 is established as shown in Fig. 6.

The angle calculation Eq. (1) can be listed from the model in Fig. 6, and the maximum cloud displacement in the y direction is obtained through the path change curve of the axis in Fig. 5, and the actual inclination angle of the axis is calculated.

$$\beta = \arcsin \frac{Y}{L} \quad (1)$$

Table 1. Material parameters of non-mechanical parts of the transmission system.

Non-mechanical parts	Material	Elastic modulus (MPa)	Poisson’s ratio	Density (kg m ⁻³)
Servo motor RV reducer	40Gr	2.12×10^5	0.277	7870
Torque sensor Magnetic powder brake	HT200	1.57×10^5	0.270	7210

Table 2. Material parameter table of the mechanical parts of the transmission system.

Mechanical parts	Material	Elastic modulus (MPa)	Poisson’s ratio	Density (kg m ⁻³)
Transmission shaft Plum blossom coupling Diaphragm coupling	Q460	2.06×10^5	0.280	7850

Table 3. The force parameter table of the transmission system model.

Model	Constraint type	Size (N)
Servo motor 1	Fixed support	250, -250
Plum blossom coupling 2-1	Cylindrical support	-2
Torque sensor 5-1	Fixed support	50, -50
Plum blossom coupling 2-2	Cylindrical support	-2
RV reducer 3	Fixed support	50, -50
Diaphragm coupling 6-1	Cylindrical support	-30
Torque sensor 5-2	Fixed support	50, -50
Diaphragm coupling 6-2	Cylindrical support	-30
Magnetic powder brake 7	Fixed support	450, -450

Table 4. Torque parameter table of transmission system model.

Transmission system	Torque	Torque value (Nm)
Input drive shaft	T_1	0.07–1.43
Output drive shaft	T_2	10–200

The calculation results are shown in Table 5. Table 5 shows the inclination angles of the input shaft and output shaft under different torque conditions when the RV reducer is actually running.

(Note that β represents the radial tilt angle of the shaft; L indicates the shaft length of the input and output ends of the RV reducer, where $L_{\text{output}} = 160$ mm, and $L_{\text{input}} = 120$ mm; and Y indicates the maximum cloud displacement value in the y direction.)

3 Establishment of coaxiality–geometric hysteresis model

3.1 Transmission ratio of RV-20E reducer

The mechanical structure of the RV reducer is shown in Fig. 7, and its transmission principle is as follows.

Sun gear no. 1, as the main input mechanism, transmits the motion to the involute planetary gear no. 2 to complete the first stage of deceleration. The planetary gear no. 2 is connected with the crank shaft no. 3 and transmits the motion of the planetary gear no. 2 to the crank shaft no. 3, and the crank on the crank shaft no. 3 drives the cycloidal gear no. 4, so that the cycloidal gear no. 4 produces eccentric motion. At the same time, the cycloidal gear no. 4 meshes with the pin gear no. 5 to make the cycloid gear no. 4 produce autorotation motion, and the autorotation motion of the cycloid gear no. 4 will be transmitted to the planet carrier (output disc no. 6) through the crank shaft no. 3 to realize constant speed output rotation, completing the second stage of deceleration.

According to Fig. 7, the transmission ratio of the RV reducer can be obtained as follows:

1. the transmission ratio of the first-stage involute planet gear,

$$i_{12}^6 = \frac{n_1 - n_6}{n_2 - n_6} = -\frac{Z_2}{Z_1}; \tag{2}$$

2. the transmission ratio of the second-stage cycloid pin gear planetary transmission,

$$i_{45}^3 = \frac{n_4 - n_3}{n_5 - n_3} = 1 - \frac{n_4}{n_3} = \frac{Z_5}{Z_4}; \tag{3}$$

3. the transmission ratio of the RV-20E reducer structure,

$$i_6 = \frac{n_1}{n_6} = 1 + \frac{Z_2 Z_5}{Z_1 (Z_5 - Z_4)}. \tag{4}$$

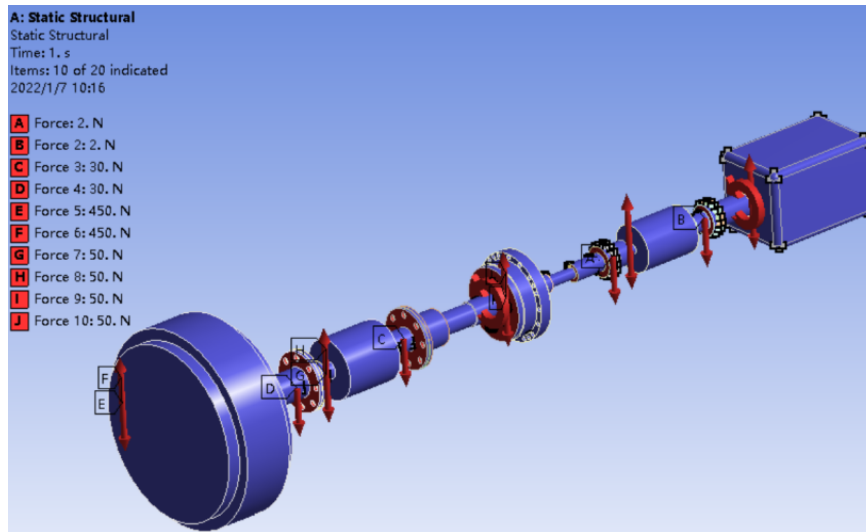


Figure 3. Boundary condition model of the transmission system.

Table 5. Radial tilt angle of transmission system model.

Input torque (Nm)	Output torque (Nm)	β_{output}	Y_{output} (mm)	β_{input}	Y_{input} (mm)
1.43	200	0.00153°	0.0042626	0.0000344°	0.000072051
1.35	190	0.00145°	0.0040486	0.0000324°	0.000067906
1.29	180	0.00137°	0.0038346	0.0000309°	0.000064796
1.21	170	0.00130°	0.0036207	0.0000289°	0.000060649
1.14	160	0.00122°	0.0034067	0.0000272°	0.000057021
1.07	150	0.00114°	0.0031927	0.0000255°	0.000053393
1.00	140	0.00107°	0.0029788	0.0000238°	0.000049765
0.93	130	0.00099°	0.0027648	0.0000220°	0.000046136
0.86	120	0.00091°	0.0025508	0.0000203°	0.000042508
0.79	110	0.00083°	0.0023369	0.0000186°	0.000038879
0.71	100	0.00076°	0.0021229	0.0000166°	0.000034733
0.64	90	0.00068°	0.0019089	0.0000149°	0.000031105
0.57	80	0.00060°	0.0016945	0.0000131°	0.000027477
0.50	70	0.00053°	0.00148105	0.0000114°	0.000023848
0.43	60	0.00045°	0.0012665	0.0000096°	0.000020215
0.35	50	0.00037°	0.0010531	0.0000076°	0.000016074
0.28	40	0.00030°	0.00083909	0.0000059°	0.000012446
0.21	30	0.00022°	0.00062512	0.0000042°	0.0000088175
0.14	20	0.00014°	0.00041115	0.0000024°	0.0000051894
0.07	10	0.00007°	0.00019718	0.0000007°	0.0000015612

In the formulas, n_1 and n_2 are the rotational speeds of the sun gear and planet gears, n_6 is the rotational speed of the output shaft (the output tray), Z_1 and Z_2 are the number of teeth of the sun gear and planet gears, n_3 and n_4 are the crank shaft and cycloid gear respectively, n_5 is the speed of the pin gear (the needle tooth shell is fixed), and Z_4 and Z_5 are the number of teeth of the cycloidal gear and the pin gear, respectively. According to the working and structural principles of the reducer, the rotation speed of the output shaft is equal to the rotation speed of the cycloid gear; i.e., $n_6 = n_4$ and $n_3 = n_2$

3.2 Coaxiality–geometric difference model of involute cylindrical gear transmission

When the RV reducer is running, the central shaft (input shaft) of the input end has a coaxiality error, and the meshing of the sun gear and the planetary gear will be affected, which will further lead to the hysteresis of the first-stage involute planetary gear transmission. For this situation, this paper takes the RV-20E reducer as an example to mathematically model the coaxiality error at the input end of the reducer. The model is as follows: the gear meshing model and

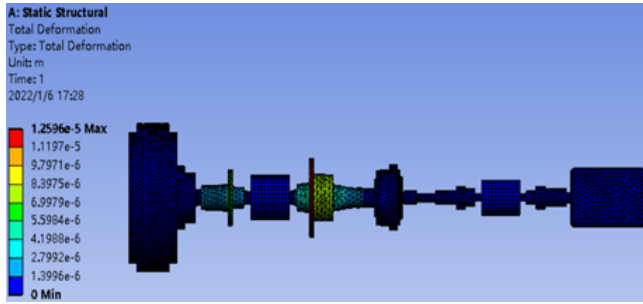


Figure 4. Simulation diagram of cloud displacement in y direction of transmission system.

the force analysis model when the input end is running normally, as shown in Fig. 8a and c, and the gear meshing model and force analysis model when there is a coaxiality error at the input, as shown in Fig. 8b and d.

When calculating the hysteresis of the involute planetary gear transmission (the first stage deceleration), the gear hysteresis caused by the average deviation of the length of the common normal is mainly considered. As shown in Fig. 8c, when the input shaft is not tilted, the hysteresis error $\Delta\phi_{12}$ is generated by the transmission of the involute gear transmission part to the output end, as shown in Eq. (5).

$$\Delta\phi_{12} = \frac{-(E_{ws} + E_{wi}) \times 180 \times 60}{2\pi r_1 i_{16} \cos\alpha_{P1}} \quad (5)$$

As shown in Fig. 8d, when the input shaft is tilted, its meshing pressure angle changes, and the new involute hysteresis error is derived as follows.

$$r_{2 \text{ pitch circle}} = (a_0 + a_1)Z_2(Z_1 + Z_2) \quad (6)$$

$$r_{2 \text{ pitch circle}} = \frac{(a_0 + a_1)Z_2(Z_1 + Z_2)}{\cos\beta} \quad (7)$$

$$v_{P2} = w_2 r_{2 \text{ pitch circle}} = \frac{w_2(a_0 + a_1)Z_2(Z_1 + Z_2)}{\cos\beta} \quad (8)$$

$$F_{tP2} = \frac{w_2^2 m_2(a_0 + a_1)Z_2(Z_1 + Z_2)}{\cos\beta} \quad (9)$$

$$F_{nP2} = \frac{F_{tP2}}{\cos\alpha_{P2}} \quad (10)$$

$$\cos\alpha_{P2} = \frac{w_2^2 m_2(a_0 + a_1)Z_2(Z_1 + Z_2)}{F_{nP2} \cos\beta} \quad (11)$$

Then the hysteresis error $\Delta\phi_{12}$ generated by the involute gear transmission part transmitted to the output end can be converted into $\Delta\phi'_{12}$, as shown in Eq. (12).

$$\Delta\phi'_{12} = \frac{-(E_{ws} + E_{wi}) \times 180 \times 60}{2\pi r_1 i_{16} \frac{w_2^2 m_2(a_0 + a_1)Z_2(Z_1 + Z_2)}{F_{nP2} \cos\beta}}, \quad (12)$$

where E_{ws} and E_{wi} are the hysteresis caused by the average deviation of the length of the common normal, r_1 is the indexing radius of the sun gear, β is the radial tilt angle of the

shaft, w_2 is the angular velocity of the planetary gear, a_0 is the center distance when the sun gear and planetary gear are in normal meshing, a_1 is the radial displacement when the sun gear and the planet gear mesh, z_1 is the number of teeth on the sun gear, z_2 is the number of teeth on the planetary gear, and m_2 is the mass of the planetary gear.

(Note that since the RV reducer is a precision instrument and the size router diameter ≤ 500 mm, it can be known that its grade is between IT1–IT5 by searching the standard tolerance table GB/T1800.1-2009, so it can be obtained that $a_1 = 0.00000075\text{--}0.0000045$ m.)

3.3 Cycloid pin wheel planetary gear drive coaxiality–geometric hysteresis

The formula for solving $\Delta\phi_{34}$ generated by the planetary transmission part of the cycloid pin gear is

$$\Delta\phi_{34} = 180 \times 60/\pi(\gamma_D + \gamma_y + \sum_{i=1}^7 \gamma_i) \quad (13)$$

$$\gamma_D = 2\Delta r_{rp}/(ez_c) \quad (14)$$

$$\gamma_y = -2\Delta r_p/(ez_c) \cdot \sqrt{1 - K_1^2}, \quad (15)$$

where Δr_{rp} is the isometric modification amount, Δr_p is the shift modification amount, e is the cycloid eccentricity, z_c is the number of cycloidal gear, and K_1 is the short width coefficient.

Since the secondary cycloid pin wheel planetary transmission belongs to the internal transmission of the RV reducer, the error caused by the tilt of its own shaft is not considered, and the basic error parameters are summed to obtain the hysteresis generated by the cycloid pin wheel planetary transmission part $\Delta\phi_{34}$, as shown in Eq. (16).

$$\begin{aligned} \Delta\phi_{34} = & \frac{180 \times 60}{\pi} \times \left(\frac{2\Delta r_{rp}}{e \cdot z_c} - \frac{2\Delta r_p}{e \cdot z_c} \right) \cdot \sqrt{1 - K_1^2} \\ & + \frac{2\delta r_p \cdot \sqrt{1 - K_1^2}}{e \cdot z_c} - \frac{2\delta r_p}{e \cdot z_c} + \frac{\delta J}{e \cdot z_c} + \frac{\Delta F_r}{2e \cdot z_c} \\ & + \frac{2\delta t \cdot K_1}{e \cdot z_c} - \frac{\Delta F_p \cdot K_1}{e \cdot z_c} + \frac{2\delta\Delta r_p}{e \cdot z_c} - \frac{2\delta\Delta r_p}{e \cdot z_c} \\ & \cdot \sqrt{1 - K_1^2} - 2K_n \cdot \delta e \end{aligned} \quad (16)$$

K_n is the center distance to produce the coefficient of hysteresis, as shown in Eq. (17).

$$K_n = \frac{\Delta r_{rp}}{e^2 \cdot z_c} - \left(\frac{z_c}{e \cdot r_p^2 \cdot \sqrt{1 - K_1^2}} + \frac{\sqrt{1 - K_1^2}}{e \cdot z_c} \right) \cdot \Delta r_p, \quad (17)$$

where Δr_{rp} is the isometric modification amount, Δr_p is the shift modification amount, δr_p is the deviation of the pin gear center circle radius, δr_{rp} is the pin gear pin radius error, δr_p is the matching clearance between the pin gear pin and the

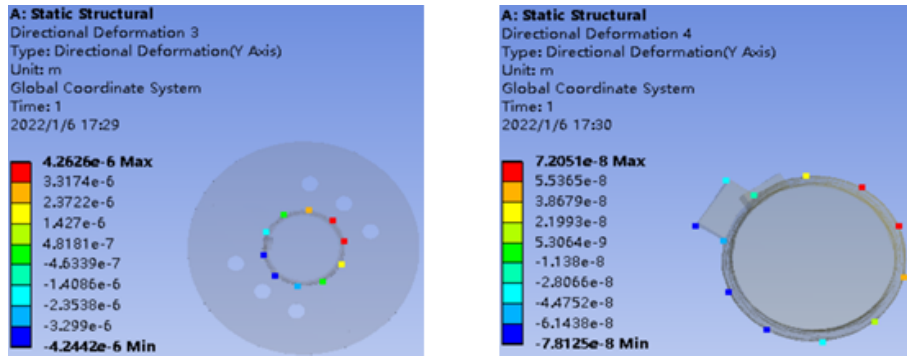


Figure 5. Cloud displacement in y direction of the transmission system.

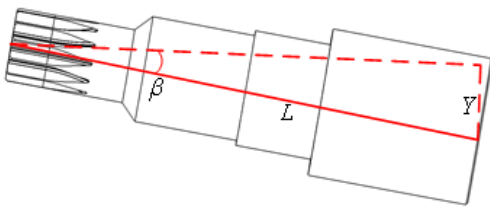


Figure 6. Input and output shaft tilt model.

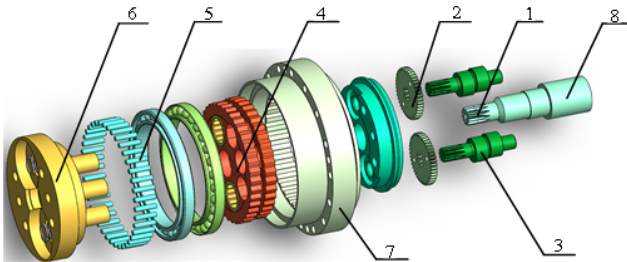


Figure 7. RV-20E reducer structure diagram: (1) sun gear, (2) planet gear, (3) crank shaft, (4) cycloid gear, (5) pin gear, (6) output disk, (7) needle tooth shell, and (8) the input shaft.

pin hole, ΔF_r is the radial circle runout error of the cycloidal gear ring, δt is the circumferential position error of the pin hole of the pin gear, ΔF_p is the cumulative error of the circumferential pitch of the cycloidal gear, $\delta \Delta r_p$ is the offset modification error, $\delta \Delta r_p$ is the shift modification error, δe is the eccentricity error, K_1 is the short width coefficient, e is the cycloid eccentricity, z_c is the number of cycloidal gear, and r_p is the radius of the pin gear.

3.4 Bearing gap coaxiality–geometric hysteresis

The swing arm bearing of the RV reducer has a certain clearance, so it will produce a corresponding hysteresis. The calculation of the hysteresis is shown in Eq. (18).

$$\Delta\varphi_{56} = \frac{180 \times 60\Delta u}{\pi a_0}, \tag{18}$$

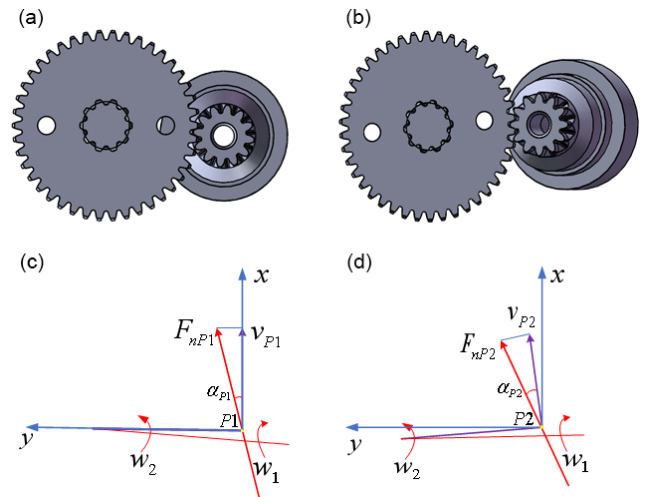


Figure 8. Actual tilt model of input shaft. (a) Normal meshing of input shaft gears (left view). (b) Input shaft gear inclined meshing (left view). (c) Normal parameter model analysis diagram (left view). (d) Analysis diagram of tilt parameter model (left view).

where Δu is the clearance of the arm bearing, and a_0 is the center distance between the planetary gear and the sun gear.

It can be seen from Fig. 9d that when the sun gear is tilted, the center distance of its gears will inevitably change accordingly, and the hysteresis $\Delta\phi_{56}$, generated by the transmission of the rotor arm bearing clearance to the output end, can be converted into $\Delta\phi'_{56}$, as shown in Eq. (20).

$$a'_0 = \frac{(a_0 + a_1)}{\cos\beta} \tag{19}$$

$$\Delta\phi'_{56} = \frac{180 \times 60\Delta u \cdot \cos\beta}{(a_0 + a_1)\pi}, \tag{20}$$

where a_1 is the radial displacement when the sun gear and the planet gear mesh, and β is the radial tilt angle of the shaft.

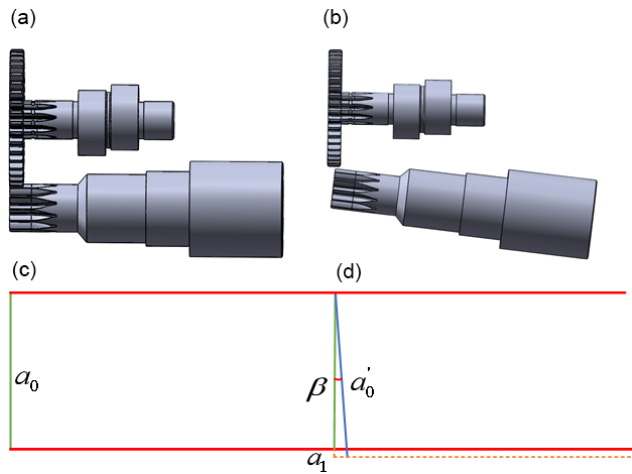


Figure 9. Actual tilt model of input shaft. (a) Normal meshing of input shaft gears (top view), (b) Input shaft gear inclined meshing (top view). (c) Normal parameter model analysis diagram (top view). (d) Analysis diagram of tilt parameter model (top view).

4 Reducer overall coaxiality–geometric hysteresis

Equations (12), (16), and (20) are added to calculate the overall hysteresis of the RV reducer, as shown in Eq. (21).

$$\begin{aligned}
 \Delta\varphi_{\Sigma} &= \Delta\varphi'_{12} + \Delta\varphi_{34} + \Delta\varphi'_{56} \\
 &= \frac{-(E_{ws} + E_{wi}) \times 180 \times 60}{2\pi r_{116} \frac{w_2^2 m_2 (a_0 + a_1) Z_2 (Z_1 + Z_2)}{F_n p_2 \cos \beta}} \\
 &\quad + \frac{180 \times 60}{\pi} \times \left(\frac{2\Delta r_{rp}}{e \cdot z_c} - \frac{2\Delta r_p}{e \cdot z_c} \right) \cdot \sqrt{1 - K_1^2} \\
 &\quad + \frac{2\delta r_p \cdot \sqrt{1 - K_1^2}}{e \cdot z_c} - \frac{2\delta r_p}{e \cdot z_c} + \frac{\delta J}{e \cdot z_c} + \frac{\Delta F_r}{2e \cdot z_c} \\
 &\quad + \frac{2\delta t \cdot K_1}{e \cdot z_c} - \frac{\Delta F_p \cdot K_1}{e \cdot z_c} + \frac{2\delta \Delta r_p}{e \cdot z_c} - \frac{2\delta \Delta r_p}{e \cdot z_c} \\
 &\quad \cdot \sqrt{1 - K_1^2} - 2K_n \cdot \delta e + \Delta\varphi'_{56} \\
 &\quad + \frac{180 \times 60 \Delta u \cdot \cos \beta}{(a_0 + a_1)\pi} \quad (21)
 \end{aligned}$$

5 Validation of geometric hysteresis model

5.1 Establishment of kinematic model based on Adams

In order to verify the accuracy of the coaxiality–geometric hysteresis model, a simulation analysis of the RV-20E reducer under no load based on Adams was conducted (Y. Tang et al., 2021; Xu et al., 2017; Wei et al., 2015), and the model establishment steps are as follows.

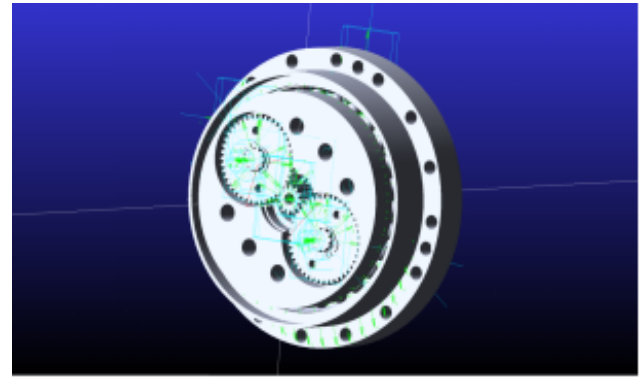


Figure 10. Interface and model in Adams.

5.1.1 Establish 3D model and import it into Adams

Firstly, the three-dimensional model of the RV-20E reducer is established through SolidWorks and then imported into Adams. The interface and model are shown in Fig. 10; the $v_{\text{input}} = 14 \text{ r min}^{-1}$ and then $v_{\text{output}} = 1 \text{ r min}^{-1}$.

5.1.2 Establishment of Adams constraints

The constraint pairs of the RV reducer kinematic model based on Adams are shown in Table 6.

5.1.3 Setting of Adams load

The impact function method (Chatterjee and Bowling, 2019) is used to calculate the contact force in the involute spur gear transmission of the RV-20E reducer. According to the Hertzian static elastic contact theory, the following equation is obtained.

$$\left\{ \begin{array}{l} K = 4R^{1/2}E/3 \\ 1/R = 1/R_3 - 1/R_4 \\ 1/E = (1 - \mu_1^2)/E_1 + (1 - \mu_2^2)/E_2 \end{array} \right\}, \quad (22)$$

where K is the stiffness coefficient ($\text{MPa mm}^{1/2}$), R_3 is the pitch circle radius of the outer gear (mm), R_4 is the pitch circle radius (mm) of the internal gear, μ_1 is Poisson's ratio of involute center gear material, μ_2 is Poisson's ratio of involute planetary gear material, E_1 is the elastic modulus of the sun gear material (MPa), and E_2 is the elastic modulus of the planetary gear material (MPa).

The calculation results show that $K = 2 \times 10^6 \text{ MP mm}^{1/2}$, and the specific parameters of contact force are shown in Table 7.

5.2 Simulation analysis of geometric hysteresis

(1) The basic size parameters of RV-20E reducer are shown in Table 8. The upper limit should be taken within the processing requirement level. The initial value of the system error parameter is shown in Table 9.

Table 6. Establishment of model constraint pairs.

Component name	Constraint type
Input shaft and ground	planar contact pair
Input axis second axis and planetary shelf	cylindrical pair
Sun gear and planet gear	planar contact pair
Crank shaft and planet gear	fixed pair
Crank shaft second-order shaft and tapered roller bearing	fixed pair
Crank shaft fourth-order shaft and needle roller bearing	planar contact pair
Crank shaft sixth-order shaft and needle roller bearing	planar contact pair
Crank shaft eighth-order shaft and tapered roller shaft	fixed pair
Cycloid gear and needle roller bearing	planar contact pair
Crank shaft and output disk	planar contact pair
Output disk second-order shaft and angular contact bearing	planar contact pair
Output disk third-order shaft and cycloid gear	planar contact pair
Pin gear and needle shell	planar contact pair

Table 7. Contact force parameter.

Parameter	Variable	Numerical value
Stiffness	K (MPa mm ^{1/2})	2×10^6
Force exponent	F_e	2.2
Damping	D (Ns mm ^{1/2})	100
Penetration depth	P (mm)	0.1
Static coefficient	μ_{still}	0.08
Dynamic coefficient	μ_{dynamic}	0.02

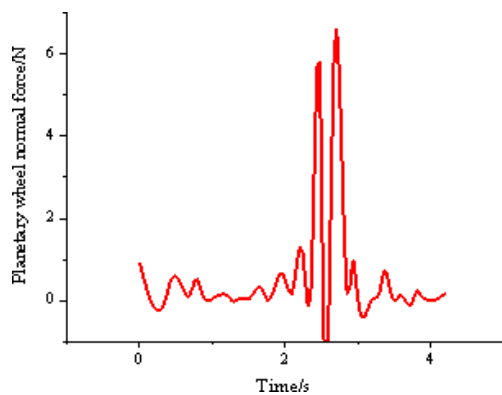


Figure 11. Sun gear circle force diagram.

(2) When the sun gear 1 of the RV reducer is engaged and the input shaft does not produce axial tilt, the normal force on the index circle of the planetary gear is obtained through Adams simulation, as shown in Fig. 11.

It can be seen from Fig. 11 that $\bar{F}_{nP2} = 0.5075$ N. Substituting the initial values of the system parameters in Tables 8 and 9 into Eq. (21), the calculation is $\Delta\phi_{\Sigma} = 0.5467$ arcmin. Since it can be seen that the hysteresis of the RV reducer is generally ≤ 1 arcmin, the model is correct.

5.3 Concentricity–geometric hysteresis model comparative analysis

Next, in conjunction with Table 5, when the RV reducer sun gear 1 is engaged and the input shaft produces a different range of axial inclination, the normal forces on the index circle of the planetary gear are obtained through Adams simulation, as shown in Fig. 12.

Figure 12 shows the normal forces of the planetary gears in the range of different axis degrees obtained by the simulation. Substitute Eq. (21) to calculate the hysteresis, as shown in Table 10.

It can be seen from Table 10 that when the coaxiality of the RV reducer transmission system exceeds the allowable error range, the hysteresis error has a tendency to continuously increase, which will make the angle data measured by the grating encoder unable to accurately reflect the accuracy of the geometric hysteresis of the RV reducer. At the same time, when the coaxiality of the RV reducer transmission system exceeds the allowable error range, the increase in the hysteresis is irregular, which may be caused by friction with the shaft.

6 Conclusions

The coaxiality–geometric hysteresis model of the transmission system of the RV reducer is established, and the model is simulated and analyzed with Adams software under the condition that the coaxiality is within different error ranges and there is no load, and the results verify the accuracy of the model. At the same time, the results show that coaxiality is one of the main factors affecting the size of the hysteresis.

The measurement method of the hysteresis of the RV reducer has not been standardized, and many influencing factors in the measurement process have not been considered. At the same time, the corresponding standards have not yet been issued, which is not conducive to the classification and

Table 8. Basic parameters of the RV-20E-141 reducer.

Parameter name	Symbol	Numerical value
Transmission ratio (the shell is fixed)	i_{16}	141
Pin gear center circle radius (mm)	r_p	52
Pin gear radius (mm)	r_{TP}	2
Eccentricity (mm)	e	0.9
Cycloid gear number	z_c	39
Number of teeth of needle gear shell	z_p	40
Number of sun gear teeth	z_1	12
Number of planetary gear teeth	z_2	42
Curtate ratio	K_1	0.72
Modulus	m	1.5
Index circle pressure angle	α	20°
Center distance between planetary gear and sun gear (mm)	a_0	27.5
Radius of sun gear index circle (mm)	i_{16}	13.5

Table 9. The initial values of the parameter error corresponding to the difference components.

Hysteresis component	Parameter error	Initial value
Geometric hysteresis of involute cylindrical gear transmission	Up deviation in length of common normal E_{ws} (mm)	0.0035
	Down deviation of common normal length E_{wi} (mm)	-0.0309
Geometric hysteresis of cycloidal pin gear drive	Isometric practice Δr_{TP} (mm)	-0.010
	Shift distance practice Δr_p (mm)	-0.012
	Needle tooth center circle radius deviation δr_p (mm)	0.010
	Pin gear pin radius error δr_{TP} (mm)	-0.004
	Matching clearance between pin gear pin and pin gear pin hole δr_{TP} (mm)	0.005
	Cycloid gear ring radial circle runout error ΔF_r (mm)	0.015
	Circumferential position error of pin tooth pin hole δt (mm)	0
	Cumulative error of cycloidal gear circumference ΔF_p (mm)	0.019
	Isometric modification error $\delta \Delta r_{TP}$ (mm)	±0.001
Shift modification error $\delta \Delta r_p$ (mm)	±0.003	
	Eccentricity error δe (mm)	0.005
Geometric hysteresis caused by bearing clearance	Crank bearing clearance Δu (mm)	0.002

Table 10. Hysteresis within the range of different axial degrees.

Radial tilt angle of output disk (°)	Radial tilt angle of input shaft (°)	Hysteresis
0°	0°	0.5462 arcmin
0.000377°	0.00000767°	0.5976 arcmin
0.000607°	0.0000131°	0.5982 arcmin
0.000837°	0.0000186°	0.6018 arcmin
0.00107°	0.0000238°	0.6029 arcmin
0.00130°	0.0000289°	0.6032 arcmin
0.00153°	0.0000344°	0.6063 arcmin

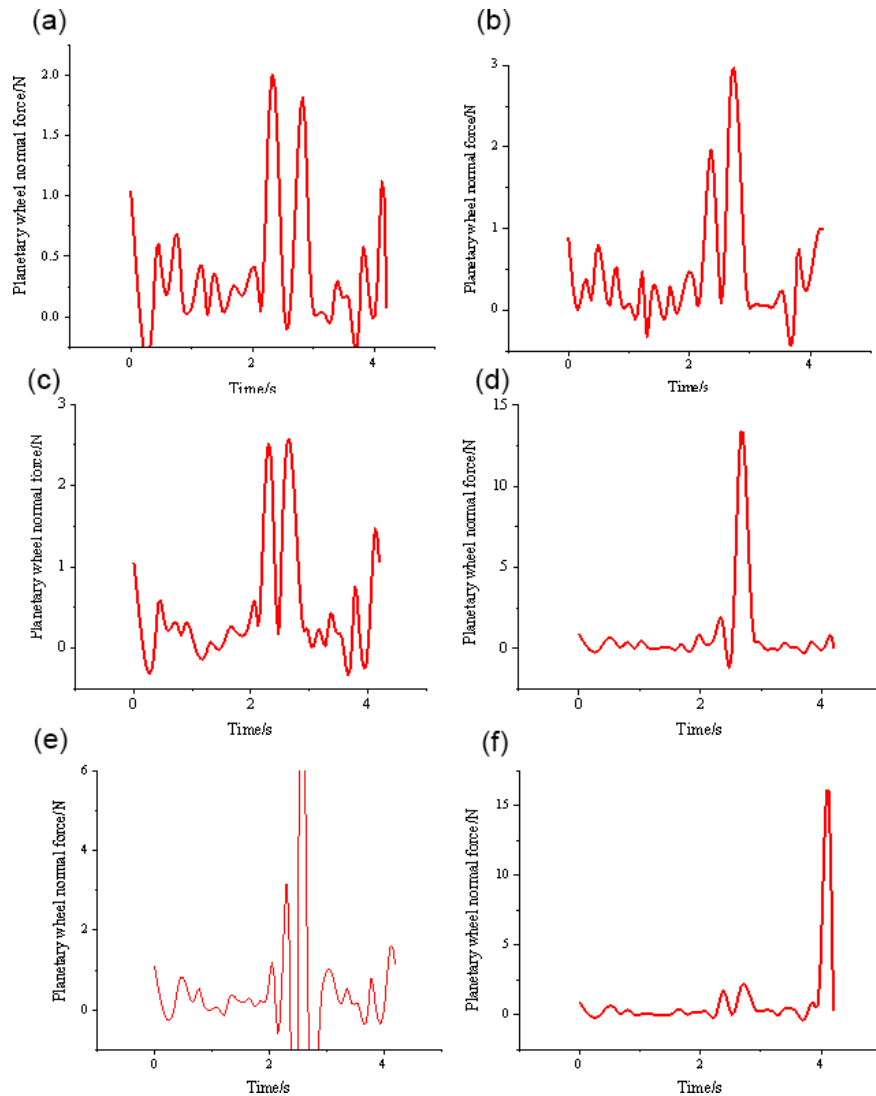


Figure 12. Planetary gear normal force within the error range of different axis degrees. (a) The input shaft is inclined at 0.00000767° . (b) The input shaft is inclined at 0.0000131° . (c) The input shaft is inclined at 0.0000186° . (d) The input shaft is inclined at 0.0000238° . (e) The input shaft is inclined at 0.0000289° . (f) The input shaft is inclined at 0.0000344° .

evaluation of the transmission accuracy of the reducer. This simulation has made a certain expansion in the categories of factors affecting the hysteresis. At the same time, it can provide theoretical basis and reference materials for the measurement and design of RV reducer hysteresis, as well as the design of RV reducer performance high-precision detection device and its adjustment mechanism, which has certain theoretical significance and practical value.

Data availability. Ansys software can be obtained from Ansys, Inc., and Adams can be obtained from the MSC Software Corporation.

Author contributions. YL is responsible for theoretical analysis and thesis writing. LF and QM conducted simulation model establishment and analysis. ZhuZ is the proposer of the theme of the thesis and the manager of the entire project. YR and ZheZ reviewed the manuscript.

Competing interests. The contact author has declared that none of the authors has any competing interests.

Disclaimer. Publisher's note: Copernicus Publications remains neutral with regard to jurisdictional claims in published maps and institutional affiliations.

Acknowledgements. Thanks are given to Guowen Ye, Shirong Zhang, and others for their help with the article.

Financial support. This research has been supported by the Anhui Polytechnic University Introduction Talent Research Start-up Fund project (grant no. 2019YQ0004), Research Project of Anhui Polytechnic University (grant no. XJKY019201905), Anhui Polytechnic University–Jiujiang District Industrial Collaborative Innovation Special Fund Project (grant no. 2021cyxtb9), Anhui Intelligent Robot Information Fusion and Control Engineering Laboratory Open project (grant no. IFCIR2020001), Overseas Research And Training Program for Outstanding Young Backbone Talents of Colleges and Universities (grant no. GXGWFX2019041), and “Research on the fluctuation wear mechanism of the modified dynamic seal ring of the disc hub motor based on dynamic multi-scale” (grant no. KJ2020A0359).

Review statement. This paper was edited by Zi Bin and reviewed by Mircea Viorel Drăgoi and two anonymous referees.

References

- Ahn, H. J., Choi, B. M., Lee, Y. H., and Pham, A. D.: Impact analysis of tolerance and contact friction on a Rv reducer using fe method, *Int. J. Precis. Eng. Man.*, 22, 1285–1292, <https://doi.org/10.1007/s12541-021-00537-7>, 2021.
- Bednarczyk, S.: Analysis of the cycloidal reducer output mechanism while taking into account machining deviations, *P. I. Mech. Eng. C-J. Mec.*, 235, 7299–7313, <https://doi.org/10.1177/09544062211016889>, 2021.
- Chatterjee, A. and Bowling, A.: Modeling three-dimensional surface-to-surface rigid contact and impact, *Multibody Syst. Dyn.*, 46, 1–40, <https://doi.org/10.1007/s11044-018-09660-2>, 2019.
- Gao, H. B., Zhuang, H. C., Li, Z. G., Deng, Z. Q., Ding, L., and Liu, Z.: Optimization and experimental research on a new-type short cylindrical cup-shaped harmonic reducer, *Journal of Central South University*, 19, 1869–1882, <https://doi.org/10.1007/s11771-012-1221-0>, 2012.
- Li, T., Tian, M., Xu, H., Deng, X., An, X., and Su, J.: Meshing contact analysis of cycloidal-pin gear in Rv reducer considering the influence of manufacturing error, *J. Braz. Soc. Mech. Sci.*, 42, 1–14, <https://doi.org/10.1007/s40430-020-2208-7>, 2020.
- Li, Y., Tong, B. A., Chen, W. B., Li, X. Y., Zhang, J. B., Wang, G. X., and Zeng, T.: Performance margin modeling and reliability analysis for harmonic reducer considering multi-source uncertainties and wear, *IEEE Access*, 8, 171021–171033, <https://doi.org/10.1109/ACCESS.2020.3023543>, 2020.
- Li, Z., Shan, J., and Gabbert, U.: A direct inverse model for hysteresis compensation, *IEEE T. Ind. Electron.*, 68, 4173–4181, <https://doi.org/10.1109/TIE.2020.2984452>, 2020.
- Pham, A. D. and Ahn, H.-J.: Hysteresis curve analysis of a cycloid reducer using non-linear spring with a dead zone, *Int. J. Precis. Eng. Man.*, 18, 375–380, <https://doi.org/10.1007/s12541-017-0045-0>, 2017.
- Qian, H. M., Li, Y. F., and Huang, H. Z.: Time-variant reliability analysis for industrial robot RV reducer under multiple failure modes using kriging model, *Reliability Engineering and System Safety*, 199, 106936, <https://doi.org/10.1016/j.res.2020.106936>, 2020.
- Su, J., Zhang, Y., and Deng, X.: Analysis and experimental study of cycloid gear form grinding temperature field, *Int. J. Adv. Manuf. Tech.*, 110, 949–965, <https://doi.org/10.1007/s00170-020-05832-7>, 2020.
- Tang, T., Jia, H., Li, J., Wang, J., and Zeng, X.: Modeling of transmission compliance and hysteresis considering degradation in a harmonic drive, *Appl. Sci.*, 11, 665, <https://doi.org/10.3390/app11020665>, 2021.
- Tang, Y., Liu, Q., and Zhu, Q.: Fault simulation and forecast of helical cylindrical gear of reducer based on Adams, *J. Phys. Conf. Ser.*, 1983, 012019, <https://doi.org/10.1088/1742-6596/1983/1/012019>, 2021.
- Tong, Q. B., Jiao, C. Q., Ning, T., and Zhang, X. D.: Harmonic gear reducer transmission error analysis and detection, *Adv. Mat. Res.*, 711, 375–380, <https://doi.org/10.4028/www.scientific.net/AMR.711.375>, 2013.
- Tran, T. L., Pham, A. D., and Ahn, H. J.: Lost motion analysis of one stage cycloid reducer considering tolerances, *Int. J. Precis. Eng. Man.*, 17, 1009–1016, <https://doi.org/10.1007/s12541-016-0123-8>, 2016.
- Wang, H., Shi, Z. Y., Yu, B., and Xu, H.: Transmission performance analysis of RV reducers influenced by profile modification and load, *Appl. Sci.*, 9, 2–19, <https://doi.org/10.3390/app9194099>, 2019.
- Wei, B., Wang, J. X., Zhou, G. W., Pu, W., Zhou, H. J., and Chu, K. M.: Mixed lubrication analysis of the main supporting angular contact ball bearing of RV reducer, *Mocaxue Xuebao/Tribology*, 35, 454–461, <https://doi.org/10.16078/j.tribology.2015.04.014>, 2015 (in Chinese).
- Xu, J. L., Yan, T., Peng, B., and Wei, B.: Effects of the transmission shaft on the main reducer vibration based on Adams and experimental demonstration, *Australian Journal of Mechanical Engineering*, 15, 2–10, <https://doi.org/10.1080/14484846.2015.1093215>, 2017.
- Yang, W., Tang, X., and Liang, Q.: Tooth surface contact analysis of involute rotate vector reducer based on a finite element linear programming method, *IEEE Access*, 7, 176719–176731, <https://doi.org/10.1109/ACCESS.2019.2955807>, 2019.
- Yu, D., Zhang, J. H., Wang, D. F., Li, X. H., and Hong, J.: Theoretical calculation and analysis on friction torque in RV reducer main bearing. *J. Zhejiang Univ. (Engineering Science)*, 51, 1928–1936, <https://doi.org/10.3785/j.issn.1008-973X.2017.10.006>, 2017.
- Zou, C., Tao, T., Jiang, G., Mei, X., and Wu, J.: A harmonic drive model considering geometry and internal interaction, *P. I. Mech. Eng. C-J. Mec.*, 231, 728–743, <https://doi.org/10.1177/0954406215621097>, 2015.